

# Towards Best Practice of Interpreting Deep Learning Models for EEG-based Brain Computer Interfaces

Jian Cui, Bin Weng

**Abstract**—Understanding deep learning models is important for EEG-based brain-computer interface (BCI), since it not only can boost trust of end users but also potentially shed light on reasons that cause a model to fail. However, deep learning interpretability has not yet raised wide attention in this field. It remains unknown how reliably existing interpretation techniques can be used and to which extent they can reflect the model decisions. In order to fill this research gap, we conduct the first quantitative evaluation and explore the best practice of interpreting deep learning models designed for EEG-based BCI. We design metrics and test seven well-known interpretation techniques on benchmark deep learning models. Results show that methods of gradient, DeepLIFT, integrated gradient, and layer-wise relevance propagation (LRP) have similar and better performance than saliency map, deconvolution and guided backpropagation methods for interpreting the model decisions. In addition, we propose a set of processing steps that allow the interpretation results to be visualized in an understandable and trusted way. Finally, we illustrate with samples on how deep learning interpretability can benefit the domain of EEG-based BCI. Our work presents a promising direction of introducing deep learning interpretability to EEG-based BCI.

**Index Terms**—Brain-computer interface (BCI), convolutional neural network (CNN), deep learning interpretability, DeepLIFT, EEGNet, electroencephalography (EEG), integrated gradient, InterpretableCNN, layer-wise relevance propagation (LRP), saliency map

## I. INTRODUCTION

A brain-computer interface (BCI) builds a direct communication pathway between the brain and external systems. It uses pattern recognition algorithms to translate brain signals into output commands. The BCI paradigms generally fall into three kinds, which are active, reactive and passive BCIs [1]. In the active BCI paradigm, users try to convey commands directly and consciously to an external device. Reactive BCIs recognize brain response in reaction to external stimulation. For passive BCIs, users' mental states are passively monitored without requiring their voluntary efforts for control.

Among the various neuroimaging techniques for BCIs, electroencephalography (EEG) is the most widely used method due to its noninvasiveness, affordability and convenience. In recent years, many efforts have been made to use deep learning models for decoding EEG signals [2]. In comparison to conventional methods based on manual feature engineering, deep learning can automatically capture essential characteristics from a large volume of data by optimizing its parameters through back-propagation and stochastic gradient

descent (SGD). It is reported that deep learning has better performance than conventional methods in many BCI domains such as identifying attentive mental state [3], movement-related cortical potential recognition [4], detection of driver drowsiness [5], etc. Despite the success, deep learning has its major drawback of lacking transparency behind its behaviors, which could raise concerns of end users on adoption of BCIs.

With the objective of enabling deep learning to explain its decisions in an understandable way to human, deep learning interpretability has become a fast-developing field in recent years [6-8]. The advances in deep learning interpretability could potentially alleviate concerns of end users and boost their trust and acceptance of BCIs. Meanwhile, the interpretation techniques can also shed light on reasons that cause a model to fail and thus facilitate the process of improving the models towards better performance. However, the topic on deep learning interpretability has not yet raised wide attention in the field of BCI. It remains unknown how accurately existing interpretation techniques can reflect the model decisions and to which extent they can benefit this domain.

In this paper, we explore the best practice of applying deep learning interpretability to EEG-based BCI. First of all, we survey existing deep learning interpretation techniques and conduct quantitative evaluations on how accurately they can interpret the deep learning models designed for EEG-based BCIs. Secondly, we investigate how the sample-wise interpretation results can be presented in an understandable and trusted way. Lastly, we illustrate by cases on how deep learning interpretability can benefit EEG-based BCI. In the following part of the paper, state-of-the-art interpretation techniques and their current applications to EEG signal classification are reviewed in Section II. Datasets and models are prepared in Section III. Existing deep learning interpretation techniques are evaluated in Section IV. Sample-wise interpretation results are analyzed in Section V, which is followed by an extensive study on the applications in Section VI. The discussion is presented in Section VII and conclusions are made in Section VIII.

## II. RELATED WORK

### A. Deep Learning Interpretation techniques

In the field of deep learning interpretability, many techniques have been proposed to interpret deep learning models by generating a contribution map (or alternatively called "relevance" or "attribution" map [9]). Each value in the contribution map indicates the importance of the corresponding pixel (or sampling point) of the input sample to the final

decision of the model. Existing interpretation techniques majorly fall into two categories – backpropagation-based methods and perturbation-based methods.

Backpropagation-based methods generate the contribution map through a single or several forward and backward passes through the network. The saliency map method [10] uses a direct way to estimate the contribution map by calculating the absolute values of gradients back-propagated from the target output. It reflects how much the target output will change when the input is perturbed locally. Zeiler and Fergus [11] proposed the deconvolution method, which modifies the back-propagation rule in the rectified linear units (ReLUs) layer – the backward gradients are zeroed out if their values are negative. By combining these two approaches, Springenberg et al. [12] proposed the guided backpropagation method which zeros out the gradients at the ReLU layer during back-propagation when either their values or values of inputs in the forward pass are negative. The gradient  $\times$  input method [13] multiplies the (signed) partial derivatives with the input sample itself. Sundararajan et al. [14] proposed the integrated gradient method, where the average gradient is computed by varying the input along a linear path from a baseline. Bach et al. [15] proposed the layer-wise relevance propagation (LRP) method which redistributes the activation values at the target neuron to the neurons connected to it according to their contributions. The redistribution process continues layer by layer until the input layer is reached. Shrikumar et al. [13] proposed the DeepLIFT method, which requires running twice forward pass with the input sample and the baseline. Similar to the LRP method, each neuron is assigned with a contribution score in a top-down manner according to the difference of activations obtained from the twice forward passes.

The perturbation-based methods only focus on the change of output by perturbation of input, while treating the network as a black box. Specifically, such methods compute the difference of output when removing, masking or altering the input sample. Zeiler and Fergus [11] proposed the occlusion sensitivity method which sweeps a ‘grey patch’ to occlude different parts of an input image and observe how the prediction changes. Similar to the method, Petsiuk et al. [16] proposed to use binary random masks to perturb the image and distribute the contribution scores among the pixels. Zintgraf et al. [17] proposed the prediction difference analysis method. They calculated the difference of a prediction by marginalizing over each feature (or pixel). Fong and Vedaldi [18] proposed to use a soft mask with continuous values to preserve discriminative regions for classification. The soft mask is optimized with various regularizations to suppress artifacts. The method was further improved by Yuan et al. [19] by using a discrete mask optimized with the generative adversarial network.

These interpretation techniques have been previously evaluated on both real [20] and synthetic [21] image datasets, as well as synthetic time-series datasets [22]. However, they have not yet been systematically evaluated on EEG datasets. In this paper, we design metrics to evaluate how accurately these techniques can interpret the deep learning models designed for EEG-based BCI.

## B. Deep learning Interpretation for EEG-based BCI

For EEG-based BCI, deep learning interpretability can reveal how different factors contained in EEG influence the model decisions. For example, Bang et al. [23] compared sample-wise interpretation by the LRP method between two subjects and analyzed the potential reasons that lead to the worse performance on one of them. The LRP method was also used by Sturn et al. [24] to analyze the deep learning model designed for a motor imagery task. They attributed the factors leading to wrong classification to artifacts from visual activity and of eye movements, which dwell in EEG channels from occipital and frontal regions. Özdenizci et al. [25] proposed to use an adversarial inference approach to learn stable features from EEG across different subjects. By interpreting the results with the LRP method, they showed their proposed method allowed the model to focus on neurophysiological features in EEG while be less affected by artifacts from occipital electrodes. Cui et al. [5] used the Class Activation Map (CAM) method [26] to analyze individual classifications of single-channel EEG signals collected from a sustained driving task. They found the model had learned to identify neurophysiological features, such as Alpha spindles and Theta bursts, as well as features resulted from electromyography (EMG) activities, as evidence to distinguish between drowsy and alert EEG signals. In another work, Cui et al. [27] proposed a novel interpretation technique by taking advantage of hidden states output by the long short-term memory (LSTM) layer to interpret the CNN-LSTM model designed for driver drowsiness recognition from single-channel EEG. The same group of authors recently reported a novel interpretation technique [28] based on combination of the CAM method [26] and the CNN-Fixation methods [29] for multi-channel EEG signal classification and discovered stable features across different subjects for the task of driver drowsiness recognition. With the interpretation technique, they also analyzed reasons behind some wrongly classified samples.

Despite the progress, it is yet not understood to which extent the interpretation results can be trusted and how accurate they can reflect the model decisions. It is also not well explained in existing work why a specific interpretation technique is chosen over others. This research gap motivates us to conduct quantitative evaluations and comparisons of these interpretation techniques on deep learning models designed for mental state recognition from EEG signals.

## III. PREPARATION ON DATASETS AND MODELS

### A. Datasets and models

#### 1) Deep learning models for EEG-based BCI

In this study, we select two benchmark deep learning models for the test. The first model is a shallow CNN named “EEGNet”, which was proposed by Lawhern et al. [4]. The model contains two blocks followed by a softmax classification layer in its structure. The first block processes the data in a temporal-spatial sequence by a standard 2D convolutional layer and a spatial depthwise convolutional layer, which was inspired by the filter bank common spatial patterns (FBCSP) algorithm [30]. In the second block, the data is further processed in the temporal dimension by a separable convolutional layer. Each block ends with a batch normalization layer, an exponential linear unit (ELU) activation layer, an average pooling layer and

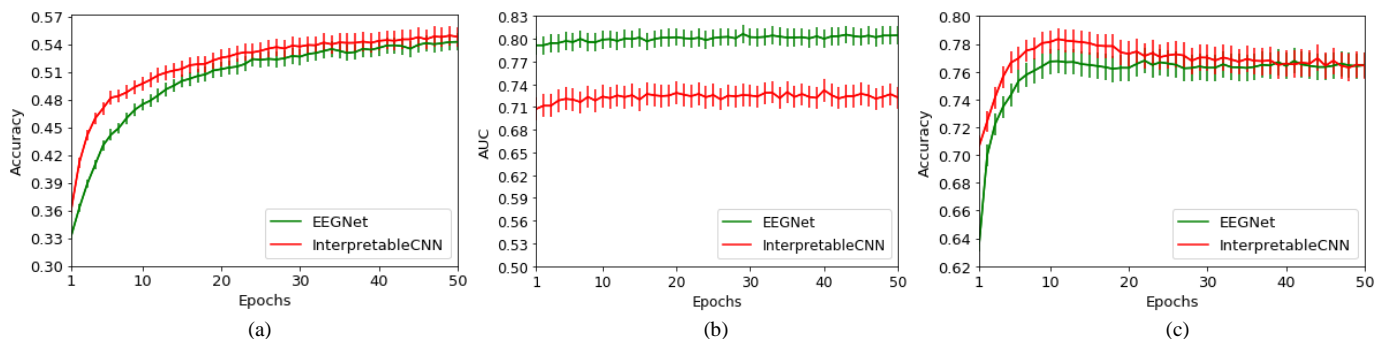


Fig. 1. Cross-subject evaluation of EEGNet and InterpretableCNN on (a) Dataset 1, (b) Dataset 2 and (c) Dataset 3 against training epochs from 1 to 50. The mean accuracies and standard errors are reported for Dataset 1 and 3, while the AUC and standard errors are reported for Dataset 2.

a dropout layer. Selection of this model in our study is motivated by the code availability and its wide application on different active and reactive BCI paradigms [4].

The second model named “InterpretableCNN” was proposed by Cui et al. [28] in their recent work for driver drowsiness recognition. The model has a compact structure with only seven layers. It processes raw EEG signals in a spectral-spatial sequence with a pointwise and a depthwise convolutional layer in the beginning, which is followed by an ReLU activation layer, a batch normalization layer, and a global average pooling layer to summarize the features. The model ends with a dense layer and a Softmax activation layer for the final classification. The model was supplemented with a novel interpretation technique based on the CAM [26] method and the CNN-Fixation method [29] for discovering meaningful patterns of EEG signals across different subjects. Selection of the model for this study is motivated by its superior performance over both conventional methods and other state-of-the-art deep learning model including EEGNet on the passive BCI domain [28].

## 2) Dataset

We select three public datasets covering the active, reactive and passive BCI domains for this study. The first two datasets were tested on the EEGNet model [4], while the third dataset was tested by authors of InterpretableCNN [28].

### Dataset 1: Sensory motor rhythm (SMR).

Motor imagery (MI) is an active BCI paradigm that decodes commands of users when they are imagining the movements of body parts [31]. It is reflected in EEG as desynchronization of sensorimotor rhythm (SMR) over the corresponding sensorimotor cortex areas. The EEG dataset comes from BCI Competition IV Dataset 2A [32]. It consists of EEG data collected from 9 subjects conducting four different motor imagery tasks, which are the imagination of moving left hand (class 1), right hand (class 2), both feet (class 3), and tongue (class 4). There are two sessions of the experiment conducted on different days for each subject. Each session consists of 6 runs separated by short breaks and each run consists of 48 trails (12 for each imaginary task). Therefore, there are in total 288 trails of a session for each subject.

The EEG data were collected from 22 channels with a sampling rate of 250 Hz. They were bandpass filtered to 0.5 Hz–100 Hz, and further processed by a 50 Hz notch filter to suppress line noise. We followed the practice in [4] to down-sample the signals to 128 Hz and extracted the EEG samples for

each trail from 0.5 to 2.5 seconds after the cue appeared. The dimension of each sample is therefore 22 (channel)  $\times$  254 (sample points).

### Dataset 2: Feedback error-related negativity (ERN)

Feedback error-related negativity (ERN) refers to the amplitude change of EEG, featured by as a negative error component and a positive component, after a subject receives an erroneous visual feedback [33]. In the experiment, ERN was induced by a P300 speller task, which is a passive BCI paradigm for selecting items displayed on the screen by detecting P300 response from EEG signals. Specifically, the subjects were asked to spell words displayed on the screen. The intention (the target letter for selection) of the subject was predicted by an online algorithm, and the prediction result was displayed as feedback on the middle of the screen after each trail. The task was to determine whether the prediction was correct by analyzing the EEG signals recorded after the subject received the feedback.

The experiment consists of five sessions. Each of the first four sessions contains 12 tasks of 5-letter word spelling, while the last session contains 20 tasks. For each subject there are 4 (sessions)  $\times$  12(tasks)  $\times$  5(letters) + 1(session)  $\times$  20 (tasks)  $\times$  5(letters) = 340 trails. 26 subjects (13 males) aged between 20 and 37 participated in the experiment. Their EEG data were recorded at 600 Hz by with 56 passive Ag/AgCl EEG sensors (VSM-CTF compatible system) placed according to a 10-20 system. The authors down-sampled the EEG signals to 200 Hz and divided them into training data (from 16 subjects) and testing data (from 10 subjects). The dataset has been made public from ‘BCI Challenge’ hosted by Kaggle [34].

We selected 32 channels out of 56 channels in our study by following the practice described in [33]. Next, we processed the data according to steps used in [4] by band-pass filtering the signals to 1–40 Hz and extracting a sample from each trail from 0-1.25 seconds after the feedback was displayed. In this way, each sample has dimensions of 32(channels)  $\times$  200(sampling points).

### Dataset 3: Driver drowsiness recognition

This dataset was built with EEG data collected from a sustained-driving experiment [35]. The subjects were required to drive a car in a virtual experiment and respond quickly to randomly introduced lane-departure events that drifted the car away from the center of the road. Their reaction time was recorded to reflect the level of drowsiness. 27 subjects (aged

from 22 to 28) participated in the experiment. The EEG signals was recorded at 600 Hz with 30 electrodes, and band-pass filtered to 1-50 Hz followed by artifact rejection.

We use pre-processed version of the dataset described in [5] for this study. Specifically, the EEG data were down-sampled to 128 Hz. A 3-second length sample prior to each car deviation events was extracted. The dimension of each sample is 30 (channel)  $\times$  384 (sample points). The samples were labeled with ‘alert’ and ‘drowsy’ according to their corresponding global and local reaction time, which were defined in [36]. The samples were further balanced for each subject and class. The final dataset contains 2022 samples in total from 11 different subjects.

### 3) Implementation

We implemented both the deep learning models with the Pytorch library. For EEGNet, our implementation is slightly different from the original model [37] in the aspect that 1) kernel regularizations were not used and 2) estimation of the computed mean and variance for the batch normalization layers was disabled (by setting `track_running_stats` as false), in order for a stable convergence on Dataset 3 [28]. The EEGNet-8,2 model, which was reported with the best performance [4], was used in this study. The source code of the InterpretableCNN model is available from [38]. The tests were conducted on the platform of Python 3.6.6. For hardware, we used an Alienware Desktop with 64-bit Windows 10 operation system powered by Intel(R) Core(TM) i7-6700 CPU and an NVIDIA GeForce GTX 1080 graphics card.

### 4) Evaluation

In this part, we evaluate the selected models on the three datasets in order to validate our implementation as well as to obtain the models with optimal parameters for interpretation. The cross-subject paradigm was carried out, in order to encourage the models to derive stable EEG features across different subject. For Dataset 1, we followed the procedures described in [32] by splitting the data collected from the first and second sessions into training and testing sets. For each time, the data from one subject collected from the second session are used as the test set, while the data of all the other subjects collected in the first session are used as the training set. The process was iterated until every subject served once as the test subject. For Dataset 2, we followed the original division of the dataset [34] by using the data from 16 subjects as the training set and the data from the other 10 subjects as the testing set. For Dataset 3, we followed the practice in [28] by conducting leave-one-subject-out cross-subject evaluation on the models.

We set batch size as 50 and used default parameters of the Adam method [39] ( $\eta = 0.001$ ,  $\beta_1 = 0.9$ ,  $\beta_2 = 0.999$ ) for optimization. Considering Dataset 2 contains imbalanced samples, we applied the weights of 1 and 0.41 (which is inverse proportion of the training data) to the “error” and “correct” classes, respectively, in the loss function. We report AUC (Area under the ROC Curve) as the performance metric for Dataset 2 and accuracies for the other balanced datasets (Dataset 1 and 3). Considering the neural networks are stochastic, we repeated evaluation of each model on each test subject for 10 times. In each evaluation, we randomized the network parameters and

trained the models from 1 to 50 epochs. The results are reported in Fig. 1.

As it can be seen in Fig. 1(a), both the models converge slowly while stably in the first 50 epochs for Dataset 1. InterpretableCNN has a slightly better performance than EEGNet and reaches its highest accuracy of 0.55 after 49 training epochs, while the highest accuracy of EEGNet is 0.54. By comparison, both of the models have a faster convergence rate on Dataset 2 – they reached their peak performance after a few training epochs at around 0.73 and 0.80, respectively for InterpretableCNN and EEGNet, as it can be seen in Fig. 1 (b). For dataset 3 shown in Fig 1 (c), InterpretableCNN reaches the peak accuracy of 0.78 after 11 epochs, which is identical to the results achieved by its original authors [28], while EEGNet also achieved a high accuracy of 0.77.

Actually, the EEGNet implemented by us has achieved higher cross-subject classification accuracy of 0.54 and AUC of 0.80 on Dataset 1 and 2 than the reported results of around 0.4 and 0.76, respectively, with its original implementation [4]. It also achieves a high accuracy of 0.77 on Dataset 3, which is around 5% higher than the results reported in [28]. InterpretableCNN has slightly higher accuracies than EEGNet on Dataset 1 and 3, while a lower accuracy on dataset 2. We inferred the performance difference was caused by the different types of average pooling layers in the two models. EEGNet uses standard average pooling layers, which makes it more sensitive to temporal features in EEG, while Interpretable CNN uses the global average pooling [40], which allows it to better capture band power features from EEG signals. We conducted an extensive test of InterpretableCNN on Dataset 2 by replacing its global average pooling layer with a standard average pooling layer. Results showed that InterpretableCNN could achieve an AUC as high as EEGNet with this modification.

The observations above validate our implementation of the selected deep learning models and their advantages on different EEG datasets.

## IV. EVALUATION ON DEEP LEARNING INTERPRETABILITY

### A. Interpretation techniques

#### 1) Statement of the problem

Suppose an EEG sample  $X \in R^{N \times T}$  ( $N$  is the number of channels and  $T$  is the sample length) is predicted with label  $c$ . The task is to generate a contribution map  $S_c \in R^{N \times T}$ , which assigns a score  $S_c(i, j)$  ( $1 \leq i \leq N, 1 \leq j \leq T$ ) to each sampling point  $X(i, j)$  indicating its contribution to the classification.

By averaging  $S_c$  over the temporal dimension, we can obtain a mean contribution map  $\bar{S}_c \in R^N$ , reflecting the average contribution of each EEG channel to the final classification. By interpolating  $\bar{S}_c$  over the whole scalp area, we can obtain a topographic map that reveals the source of signals that contain important features.  $\bar{S}_c$  has been widely used in existing work [23, 25, 28] to interpret the classification results. In this paper, we name  $\bar{S}_c$  as “channel contribution map”.  $S_c$  is called “contribution map” or alternatively “sample contribution map”, referring to the map generated for the whole sample.

## 2) Interpretation techniques and implementation

Following the review in Section II.A, we narrow down existing deep learning interpretation techniques for our study with the following criteria. 1) The interpretation techniques to be investigated in this study are expected to be applicable to deep learning models with different structures. This exclude the methods that designed for a specific model, e.g., [26, 28, 41]. 2) In order to allow the results reported in this paper to be reproducible, the selected interpretation techniques are expected to produce identical results for the same sample after each run. We therefore exclude methods that use random initialization of parameters, e.g., [16, 42]. 3) The selected interpretation techniques are expected to have minimal adjustable parameters, so that the results cannot be manipulated by fine-tuning of the parameters. The techniques with parameters that significantly influence the results are excluded, e.g., [18]. 4) The selected interpretation techniques are expected to be computationally efficient. The methods that have a low computation speed are excluded, e.g., [43, 44].

Most of the interpretation techniques that meets the listed criteria belong to the back-propagation methods, while the perturbation-based methods are either computationally inefficient or have many adjustable parameters that can significantly influence the results [18]. Based on the observation, we select seven back-propagation based methods for our initial test and they are the saliency map [10], deconvolution [11], guided backpropagation [12], gradient $\times$ input [13], integrated gradient [14], LRP [15] and DeepLIFT [13].

The selected interpretation methods were implemented for EEGNet and InterpretableCNN with the Pytorch library. We used the input sample with zero entries as baselines [9] for integrated gradient and DeepLIFT. We computed the average of gradients generated from the path between the baseline and the input with 100 steps for the integrated gradient method. We implemented the LRP with  $\epsilon$ -rule and DeepLIFT with rescale-rule by modifying the gradient flow in the nonlinear activation layers (the ReLU activation layer for InterpretableCNN and three ELU activation layers for EEGNet) with the method proposed by Ancona et al. [9]. LRP is equivalent to gradient  $\times$  input for InterpretableCNN as the model only has ReLU activation for the nonlinear layer [9]. In order to remove the influence of other samples from the same batch on the interpretation results, we made the batch normalization layers behave linearly by fixing the parameters of batch mean and standard deviation during back-propagation. The parameters were obtained from an additional forward pass of the tested batch data.

## B. Evaluation metrics

According to [45], existing methods for evaluating deep learning interpretability fall into two categories: human-dependent and human-independent. The first category of methods rely on human efforts in the evaluation process or directly let a person evaluate the explanations [46, 47]. For example, the contribution maps were compared with “ground truth” regions labeled by humans for an image classification task [18]. The second category of methods rely on objective metrics without human intervention. Considering the EEG data are mostly complex and difficult to be interpreted by human,

we designed tests belonging to the second category to evaluate the interpretation techniques for both sample and channel contribution maps.

### 1) Sensitivity test

Our first test was inspired by the sensitivity- $n$  test proposed by Ancona et al. [9]. In the method, they randomly perturbed  $n$  pixels (by setting their values to zeros) from the input sample and observed change of output. Ideally, the sum contribution of the  $n$  points is proportional to the change of model output. They varied  $n$  from 1 pixel to about 80% pixels and calculated Pearson correlation coefficient (PCC)  $r$  for each  $n$  as the quality metric of the contribution map.

Our test is different in the aspect that we perturbed the input sample locally by small patches with fixed size  $n$  instead of  $n$  random points from different parts of the sample. In this way, we can evaluate local accuracy of the contribution map while introducing less high-frequency noise to EEG signals. We limit the patch size  $n$  to 0.1-0.5 of the sample length, which correspond to 0.45%-2.27%, 0.31%-1.56%, and 0.33%-1.67% of the sample size for Dataset 1, 2 and 3, respectively. We assume the perturbation will not significantly drift the sample away from its original distribution. For each  $n$ , we randomly perturbed the sample 100 times and calculate the correlation coefficient as a quality metric of the contribution map.

The channel contribution map was evaluated with a single correlation coefficient, which is obtained by perturbing each channel once.

### 2) Deletion test

Despite the sensitivity test can measure accuracy of a contribution map, it does not indicate how the interpretation result is associated with the model prediction. Therefore, the deletion test proposed in [16] is used in this study. In this test, we ranked the sampling points of the input sample in a descending order according to their scores in the contribution map. By varying  $n$  from 1%, 2%, ..., 100% of the sample size, we calculated the probabilities of the predicted class when the first  $n$  points were removed from the sample by setting their values to zeros. A sharp drop of the probability on the predicted class, or alternatively a small area under the probability curve (as a function of  $n$ ) is indicative of a high-quality contribution map.

We performed the deletion test for the channel contribution map in a similar way – each time we removed a channel by setting them to zeros and calculated the probability of the predicted class.

## C. Test settings

Dataset 1 contains EEG data collected from 9 subjects. Each subject has 288 training samples and 288 testing samples with balanced 4 classes. We randomly selected 25 samples for each class from the test samples of each subject. In this way, we have in total 9 (subjects)  $\times$  4 (classes)  $\times$  25 (samples) = 900 samples for evaluating the interpretation results. In the leave-one-subject-out evaluation paradigm, we trained EEGNet and InterpretableCNN with 49 epochs in order to achieve the best performance.

Dataset 2 contains EEG data collected from 16 training subjects and 10 testing subjects. Each subject has samples with

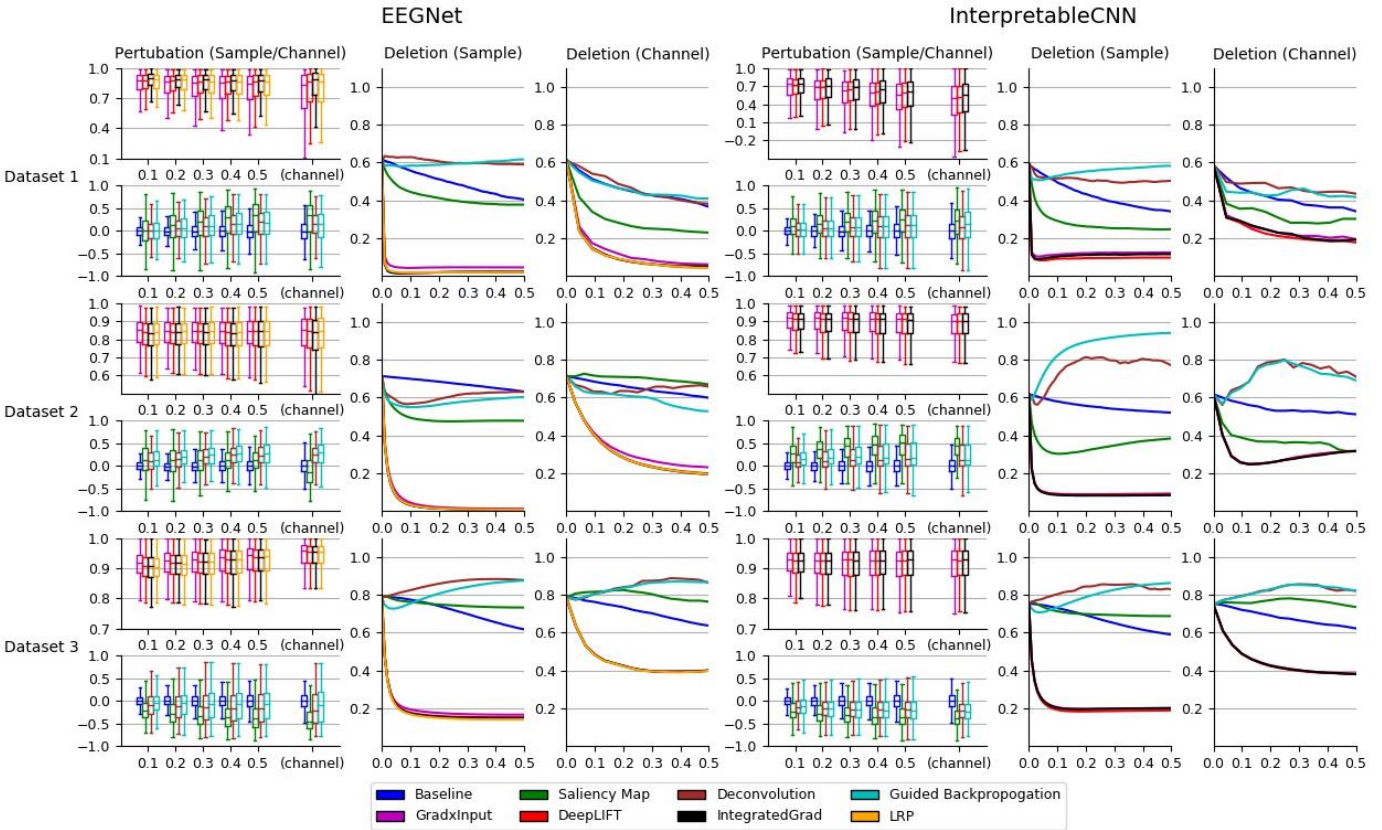


Fig. 2. Evaluation results of the interpretation techniques for InterpretableCNN and EEGNet on the three datasets. The results for EEGNet and InterpretableCNN are displayed in columns 1-3 and columns 4-6, respectively. The results for the three datasets are displayed in the three rows, respectively. The sensitivity test results are shown in column 1 and 4. We display the boxplot of the correlation coefficients  $r$ , which is in the range of -1 to 1 (1 represents a perfect correlation). The sensitivity test results for both the sample and channel contribution maps are displayed in the same sub-figure while different interpretation techniques are grouped and separately displayed in two sub-figures. For InterpretableCNN, results for the LRP method are not shown since they are identical to that obtained with the gradient

unbalanced labels. We selected 100 samples from each test subject and thus have in total 10 (subjects)  $\times$  100 (samples) = 1000 samples for evaluation. For the test subjects 1-6, 9 and 10, we randomly selected 50 samples of each class from each subject. For subjects 7 and 8 with less of 50 samples for the class of error feedback, we used all the samples from this class and randomly selected the rest samples from the class of correct feedback. We trained EEGNet and InterpretableCNN model with 10 epochs for evaluation.

Dataset 3 contains EEG data collected from 11 subjects. We randomly selected 50 samples of each class from each subject, and thus have in total 11 (subjects)  $\times$  2 (classes)  $\times$  50 (samples) = 1100 samples for evaluation. We trained the EEGNet and InterpretableCNN models with 11 epochs for evaluation in order to achieve the best performance on this dataset.

For each sample, we generated a contribution map with random values as baseline. The corresponding channel contribution map is obtained by averaging the sample contribution map over the temporal dimension.

#### D. Results

As it can be seen from the results displayed in Fig. 2, the interpretation techniques can be divided into two groups according to their performance in the tests. The first group of methods, consisting of gradient

gradient, and LRP, have similar and better performance than the second group of methods consisting of saliency map, deconvolution and guided backpropagation. In the sensitivity test, the correlation coefficients obtained with the second group of methods have median values at around zero under different conditions, which is similar to the baseline method using randomly generated contribution maps. In the deletion test, the second group of methods mostly have large AUC (Area under the Curve), indicating the most important features learned by the deep learning models for classification are not accurately localized. By comparison, the first group of methods have better performance than the baseline and the second group of methods in the two tests. In the deletion tests, it can be observed that a low probability on the predicted class (below 0.2 under all the conditions) is reached when less than 0.1 portion of the total data are removed from a sample, indicating a small portion of features that contribute most to the classification have been successfully localized. In the sensitivity test, all the median values of correlation coefficients obtained under different conditions are higher than baseline.

According to the results, the methods of gradient

interpretation results is not consistent for every sample despite when the best available interpretation techniques are used, as it can be observed for the case of Dataset 1 that the correlation coefficients obtained with the first group of methods have a wide range. The individual interpretation results should therefore be cautiously treated, since they could be uninformative or even misleading for many samples. We further investigate this problem and look into individual cases in the next section.

There are also some other interesting findings revealed by the test. For example, in the sensitivity tests we can observe that the performance of second group of methods are improving along with increase of the perturbation patch sizes for InterpretableCNN on Dataset 3, while it is the opposite for the same model on Dataset 1. This could be caused by the different types of features appearing EEG with different durations in these two datasets. Limited by the scope of the paper, we leave further investigation of such interesting phenomena to future work.

### V. SAMPLE-WISE INTERPRETATION AND ANALYSIS

The contribution maps are commonly visualized as heatmaps [26, 41] or colormaps [5, 27, 28] by mapping the values to colors after normalization. We show a concrete sample in Fig. 3 in order to illustrate the problem we meet with the standard way of visualization and discuss how it can be improved with our proposed processing pipeline. The sample is obtained from Dataset 3. It is predicted correctly with the label of drowsiness by InterpretableCNN with probability of 1, indicating that features strongly correlated with the drowsiness have been identified by the model. The sample contains apparent alpha spindles in its first half part (around 0-1.5 seconds), which were found to be a strong signal of drowsiness [5]. The contribution map is obtained with the  $\text{grad} \times \text{input}$  method, and it is visualized in Fig. 3(a) as a colormap directly after normalization. However, it is difficult to observe any meaningful pattern from the contribution map, as it is corrupted by the heavy high-frequency noise. Actually, we would expect to observe distinguishable features from FCZ, CZ, CPZ and FT7 channels, as which are highlighted in the topographic map. In this connection, we propose the following steps for processing the contribution maps in order to make the features clearly visible.

**Step 1 – Normalization.** As it is used in the standard procedure, the contribution maps are normalized in the first step by subtracting the mean and dividing by the standard deviation. This operation is conducted on both the sample and channel contribution maps.

**Step 2 – Thresholding.** One of the major reasons that make the contribution map look noisy is that too much information, including all of the positive, neutral and negative pixels with relation to the predicted class, is displays simultaneously in the sample picture. However, what really of interest are only the small portion of the positive areas that contribute most to the classification. In order to reduce the abundant information and make the target features distinguishable, we manually set a threshold and remove the unnecessary information from the normalized contribution map below this threshold. Technically, this operation is performed by subtracting the threshold from

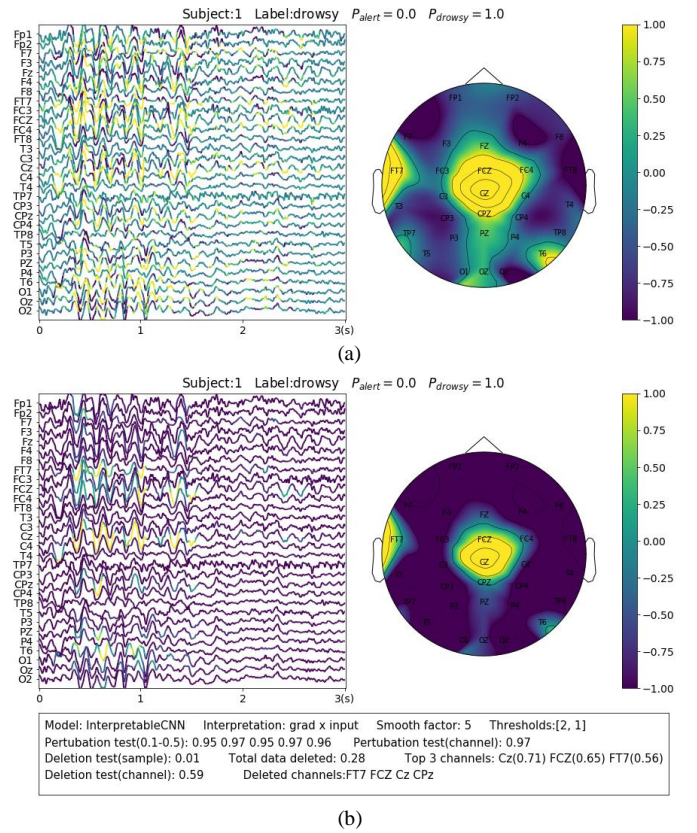


Fig. 3. Comparison of the contribution maps visualized (a) simply after normalization and (b) after processing with the proposed pipeline for a sample selected from Dataset 3. The subject ID, ground truth label, probabilities of both classes are shown on the top of each sub-figures. The contribution scores are converted to colors overlaid on the signals. An evaluation report is generated and attached below the instance in (b). In the report, the deep learning model, the interpretation technique, the smoothing window size and the thresholds (for the sample and channel contribution maps) are displayed in the first line. The perturbation testing results for the sample and channel contribution maps are displayed in the second line. The deletion test results for the sample and channel contribution maps are displayed in the third and fourth lines, respectively. The first item in the third line shows the new probability after deleting the highlighted parts of the signal. The second item shows the total amount (portion) of data deleted. The third item shows the top 3 channels that contain the most of the deleted data and the amount (portion) of deleted data from them. In the fourth line, the first item shows new probability after deletion of the channels listed in the second item.

the contribution map obtained from the previous step and setting its values as the lower bound of the color map (which is -1 for our case) if they are below it. This operation is performed on both the normalized sample and channel contribution maps. The thresholds can be adjusted (we empirically set them in the range of 0-1) to achieve the desired visualization.

**Step 3 – Smoothing.** Most of the noise contained in the contribution maps can be effectively removed by the previous processing step. The most important features left can form into local patches and thus be clearly distinguishable after smoothing in the temporal dimensional. Our empirical results show that the desired visualization can be achieved by applying an averaging moving window with a small length in comparison to the whole length of the signal, in which case the local sensitivity of the contribution maps can be largely preserved at the same time.

Coming back to the sample shown in Fig. 3, we preformed the proposed processing steps with the thresholds of 2 and 1 for

the sample and channel contribution maps, respectively, and the smoothing window with size of 5. As it can be seen in Fig. 3(b), the visualization is apparently improved – the alpha spindle features are clearly visible from the channels of FCZ, CZ, CPZ and FT7, which is consistent with the information revealed from the topographic map.

However, the contribution maps themselves cannot reflect how well the model decisions are interpreted, even when they seem to be plausible and convincing (we show an example to support this assertion in Fig. 4). Considering the quality of interpretation cannot be guaranteed despite when the best available interpretation techniques are used (as observed in the previous section), it is therefore important to conduct sample-wise evaluation and present the results along with the interpretation. To keep the consistency of the paper, we use the sensitivity and deletion tests as described in Section IV. B for the evaluation. The sensitivity test is conducted on the original contribution maps (before processing Step 1) to reflect the best correlation achieved between the perturbed batches and the model output. This is because we deliberately remove (in processing Step 2) and alter (in processing Step 3) the information contained in the original contribution map in order to enhance the visualization, which will definitely affect the sensitivity test results. The deletion test is conducted on the processed contribution map (after processing Step 3) – we remove the highlighted areas (for the contribution map) or the channels (for the sample contribution map) and the report the probability output by the model on the predicted class. In this way, the deletion test results can be directly related to what is observed from the displayed colormap. We generate the evaluation report in the text box under each figure.

We display another two samples in Fig. 4 for the purpose of illustration on the importance of sample-wise evaluation. The input sample is from Dataset 1 and it is labeled with “both feet”. It is wrongly classified with the “tongue” label by both EEGNet (shown in Fig. 4 (a)) and InterpretableCNN (shown in Fig. 4 (b)). The DeepLIFT method is used to interpret the results of both models and the colormaps are generated with the proposed processing pipeline. By observation on the interpretation results, we can notice that similar patterns have been identified—the features that contribute most to the classification are majorly from the signals recorded at around 0.75-1 second. The channels of CP3 and CP1 play important roles for the prediction. However, the quality of the interpretation results are completely different between the two samples. The correlation coefficients obtained from the sensitivity test fall in the range of 0.74-0.89 for the first sample shown in Fig. 4 (a), while they are in the range of 0.09-0.59 for second sample shown in Fig. 4 (b). Removal of the highlighted regions (taking up 0.07 of total data) of the first sample will cause the probability drop from 0.5 to 0.0, while removal of the highlighted regions (taking up 0.06 of total data) of the second sample will only cause the probability drop from 0.6 to 0.4. Removal of the channel (CP1) with the highest contribution for the first sample will cause the probability drop from 0.5 to 0.45, while removal of the most important channel (CP3) for the second sample will cause the probability on the contrary increase from 0.6 to 0.98 for the second sample.

The case displayed in Fig. 4 illustrates the importance of sample-wise evaluation, without which it is easy to draw biased

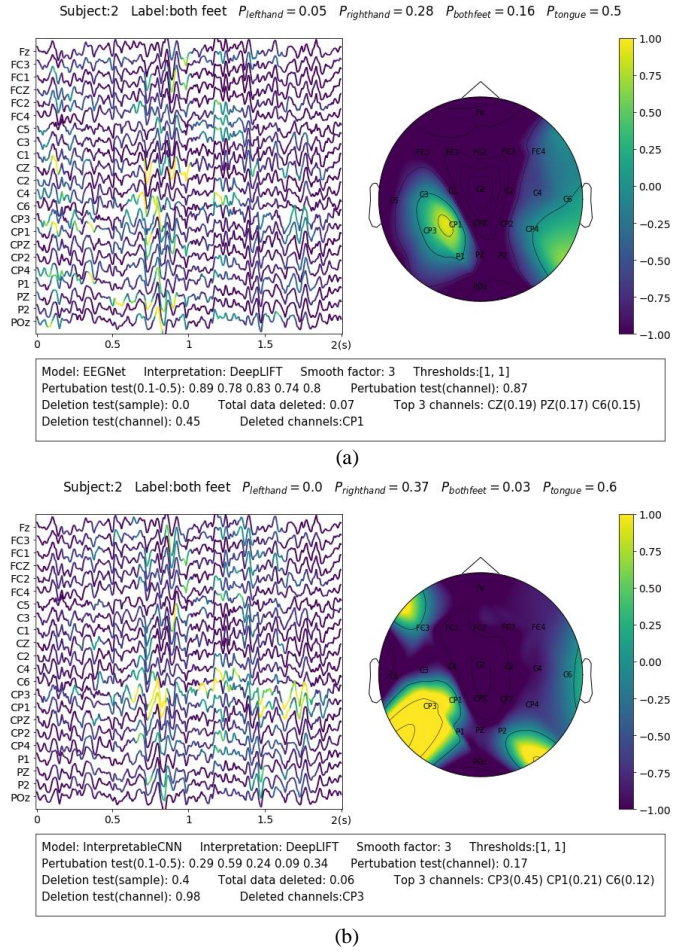


Fig. 4. Comparison of the interpretation results on a sample classified by (a) EEGNet and (b) InterpretableCNN. The contribution maps generated for the two samples display similar patterns, while the qualities of the interpretation results vary greatly as revealed by the evaluation report.

conclusions from the misleading interpretation results. Despite some factors that could potentially influence the quality of interpretation can be observed from the obtained results, e.g., the deep learning model structures and the different types of EEG features, it is yet not fully understood what actually lead to failure of interpretation for some samples, e.g., the one in Fig. 4(b). We leave further investigation on this topic to future work and avoid using such cases for illustration in this paper.

## VI. APPLICATION

In this section, we extensively explore how we can benefit from sample-wise interpretation of deep learning models for EEG-based BCI. The applications are explored in two scenarios. In the first scenarios, we visualize the neurophysiological features learned by the models from EEG for different datasets, which is an important step of model validation. In the second scenario, we show the advantages of using interpretable deep learning to discover different types of noise and artifacts in the datasets and discuss how the classification accuracy can be potentially improved based on the findings.



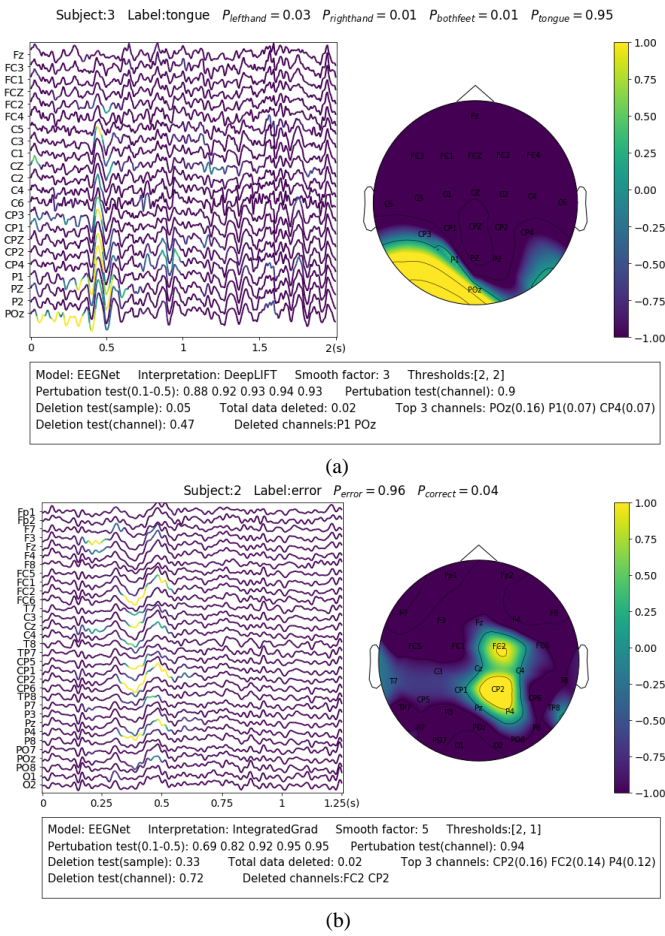


Fig. 5. Visualization of the learned neurophysiological features from two samples. The first sample (a) is from Dataset 3 and the second sample (b) is from Dataset 2.

### 1) Visualization of neurophysiological features

Deriving insights into what the model has learned from the data is an initial step of model validation. The interpretation results allow us to know whether neurophysiological features have been learned from the data to distinguish different mental states. We have selected three representative samples from the three datasets, respectively, for the purpose of illustration.

For the SMR dataset (Dataset 1), the samples were collected while the subjects are imaging movements of different body parts. This reflects in EEG as event-related desynchronization (ERD) during imagination and event-related synchronization (ERS) after imagination of sensorimotor rhythm (SMR) or Mu rhythm (8-13Hz) over the corresponding sensorimotor cortex areas [48]. A representative sample is shown in Fig. 5 (a). The sample is correctly predicted with label of “tongue movement” by EEGNet with probability of 0.95. From the topological map, we can observe that the model has found important features from P1 and POZ channels, which are closest to the sensorimotor area of the tongue [49]. From the sample contribution map, it can be observed that the model has recognized the decreased amplitude sensorimotor rhythm (or ERD) at around 0-0.4 seconds from POZ channel, as well as an instant burst of Mu spindles at around 0.4-0.6s as evidence for the prediction. The amplitude change of SMR reflects neuron activities resulted from the tongue imagination task in the corresponding sensorimotor area.

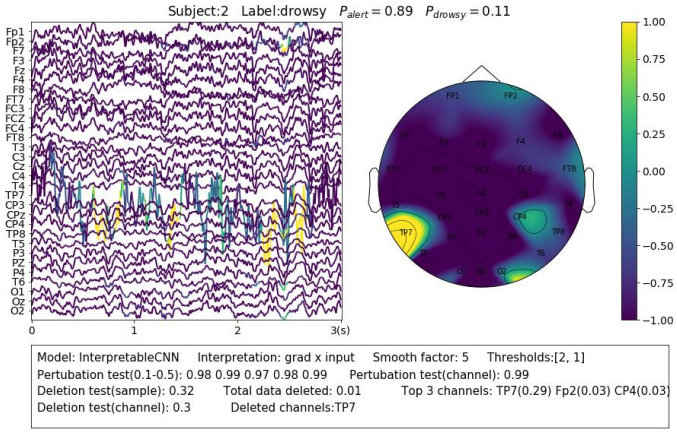
Feedback related negativity (FRN, or feedback ERN) refers to a specific kind of evoked responses produced by the brain when negative feedbacks are received from external stimuli. It is featured by a negativity peaking of EEG signals around 250 ms after feedback is presented [50]. For Dataset 2, FRN occurs when the subject receives error prediction of the letter displayed on the screen. As it can be seen in the example shown in Fig. 5 (b), the model has identified the typical FRN feature, which has a negativity peaking followed by a positive peaking (see Figure 7 in [33]), at 0.25-0.5s after the feedback is presented. The sample is predicted with the “error” class with probability of 0.96. Removal of the highlighted areas (taking up 0.02 of total data) will cause the probability to drop from 0.96 to 0.33. The identified feature appears in several EEG channels simultaneously, so that removal of the most important two channels FC2 and CP2 will only cause the probability to drop from 0.96 to 0.72.

For Dataset 3, Alpha spindles, which are characterized with an arrow frequency peak within the alpha band and a low-frequency modulation envelope resulting in the typical ‘waxing and waning’ of the alpha rhythm [51], are the most notable features in EEG associated with drowsiness [28]. A typical sample is shown in Fig. 3(b). The sample is predicted correctly by InterpretableCNN with probability of 1.0. The Alpha spindle features have been identified by from several episodes of the signal majorly in the central cortical areas. Removal of the features (taking up 0.28 of total data) will cause the probability to drop from 1.0 to 0.28.

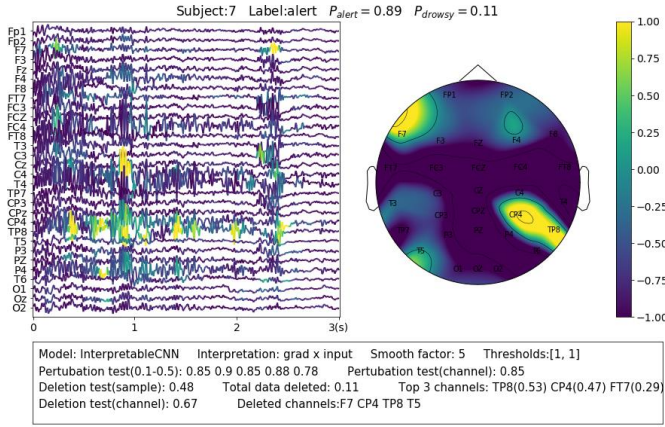
### 2) Discriminating different noises and artifacts

EEG recording is highly susceptible to various forms and sources of noise and artifacts. The sensor noise contained in EEG is one of the major reasons that affect the model decisions. Interpretable deep learning allows us to understand how different kinds of sensor noise impact the model decisions. We selected two samples from Dataset 3 for illustration. The first sample shown in Fig. 6 (a) contains apparent sensor noise in TP7 channel. The model falsely identified several local regions of the sensor noise as evidence for decision. The significant amplitude changes of the signal in TP7 channel could be caused by loose conduct between the sensor and skin. Such kind of sensor noise that seriously affects the model decision should be cleaned from the data. The second sample shown in Fig. 6 (b) contains heavy high-frequency noise in several EEG channels, e.g., CP4. The model identifies several regions from the noise areas as evidence for classification. Actually, we have observed many samples containing similar noise in the dataset that are correctly classified with alert labels, which indicates that this kind of noise could have a strong relationship with the alert state. The noise is actually caused by electromyography (EMG) activities resulted from tension of scalp muscles. They usually dominate the wakeful EEG signals [52] and become the most apparent feature of alertness [5, 27, 28], while the cortical source Beta activities with very low amplitude [53] in wakeful EEG are not as easy to be distinguished.

Eye blinks and movements are another common source of artifacts in EEG signals. Interpretable deep learning allows us to identify samples that contain such kind of artifacts and understand how they affect the model decision. For Dataset 2, we find there are many samples, similar to the case shown in



(a)

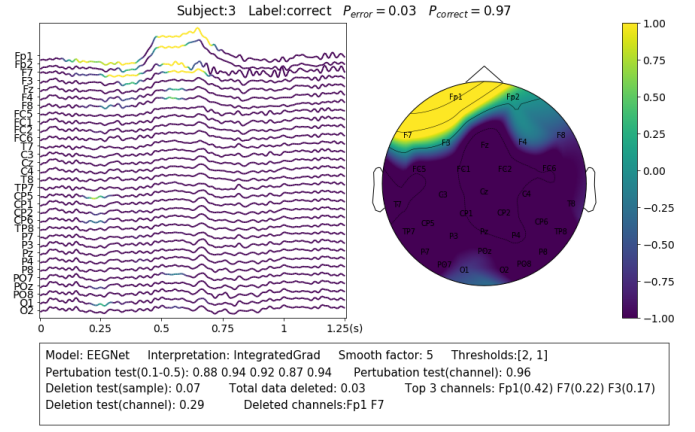


(b)

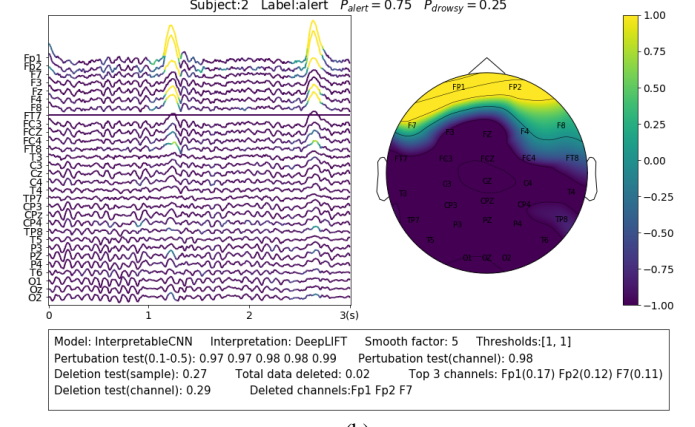
Fig. 6. Visualization of the interpretation results for selected samples containing different types of noise.

Fig. 7 (a), containing the eye blink artifacts while they are identified by the model as evidence of the “correct” class. The eye blinks could be a sign of relief after the subjects stare at the screen with high concentration in the P300 task. Such class-discriminative artifacts should be removed from the dataset and the model is expected to learn EEG features (e.g., ERP) generated from cortical sources instead. However, the case is on the contrary for Dataset 3, where the eye blink and movement features are overly cleaned. Actually, the rapid eye blinks, as reflected in EEG a short-term pulse in the frontal channels (Fig. 7 (b)), are indicators of the alert and wakeful state. They have been found by deep learning models as important features for classification [28]. However, the eye blink and movement features are overly cleaned in the pre-processing phase for Dataset 3, which causes the prediction accuracy to drop around 0.3 for Subject 2 in our test. We show in Fig. 7 (b) an uncleaned sample from subject 2 and it can be seen that model has made the right prediction based on such kind of features. Removal of the features will cause the model to make the wrong prediction.

The observations above lead to the conclusion that different type of noise should be treated differently rather than indiscriminately removed from EEG signals. The noise and artifacts defined in one scenario could become important features in another scenario. Interpretable deep learning provide us with the advantage of understanding how they impact the



(a)



(b)

Fig. 7. Visualization of the interpretation results for two samples containing eye blink artifacts

model decisions so that we can take proper strategies accordingly to deal with them.

## VII. DISCUSSION

In this paper, we investigated the topic of applying deep learning interpretability to EEG signal recognition. Despite the wide application of deep learning, there are yet no guidelines or recommendations on how to interpret the results, what methods should be used and how accurate they can reflect the model decisions for EEG-based BCI. In order to fill this research gap, we conducted quantitative studies to evaluate existing interpretation techniques and explored the best practice of interpreting deep learning designed for EEG signal recognition.

The results revealed the importance of selecting a proper interpretation technique in the first step. Existing interpretation techniques, e.g., the saliency map method, despite being widely used in existing work for interpreting learned EEG patterns [54], could actually fail to outperform baseline with randomly generated contribution maps in certain circumstances. In addition, we also find that the quality of the interpretation results is inconsistent for individual samples despite when a method with an overall good performance is used. Many factors, including model structure and types of features in the samples, could potentially affect the quality of the interpretation results. It is therefore recommended to conduct sample-wise evaluation to validate the results. By far as we know these

findings not yet raised wide awareness in work interpreting deep learning for EEG-based BCI, e.g., [24, 25].

In order to make the interpretation results understandable, we proposed a few processing steps that can effectively enhance the visualization. Furthermore, we extensively used interpretable deep learning to explore how different types of noise and artifacts in the datasets can affect the model decisions. Our analysis leads to the conclusion that different types of noise and artifacts should be treated differently based on a comprehensive understanding of the overall pattern learned from the dataset. The noise and artifacts defined in one scenario could become important features in another scenario. Interpretable deep learning could be potentially used as a powerful tool to discover the patterns underlying a dataset, so that a proper strategies can be specifically designed in the pre-processing pipeline.

### VIII. CONCLUSION

In this paper, we explored the best practice of applying deep learning interpretability to EEG-based BCI. Firstly, we surveyed existing deep learning interpretation techniques and shortlisted seven of them that can be applied to deep learning models with different structures. We designed evaluation metrics and tested them with two benchmark deep learning models on three different EEG datasets. The results showed that the methods of gradient, DeepLIFT, integrated gradient, and LRP have higher accuracies than that of saliency map, deconvolution and guided backpropagation methods for interpreting deep learning models. Secondly, we proposed a series of processing steps that allow the sample-wise interpretation results to be presented in an understandable and trusted way. Lastly, we used examples to illustrate how deep learning interpretability can benefit EEG-based BCI. Our work illustrates a promising direction of using deep learning interpretability to discover meaningful patterns from complex EEG signals.

### REFERENCES

1. Hramov, A.E., V.A. Maksimenko, and A.N. Pisarchik, *Physical principles of brain-computer interfaces and their applications for rehabilitation, robotics and control of human brain states*. Physics Reports, 2021.
2. Roy, Y., et al., *Deep learning-based electroencephalography analysis: a systematic review*. Journal of neural engineering, 2019. **16**(5): p. 051001.
3. Fahimi, F., et al., *Inter-subject transfer learning with an end-to-end deep convolutional neural network for EEG-based BCI*. Journal of neural engineering, 2019. **16**(2): p. 026007.
4. Lawhern, V.J., et al., *EEGNet: a compact convolutional neural network for EEG-based brain-computer interfaces*. Journal of neural engineering, 2018. **15**(5): p. 056013.
5. Cui, J., et al., *A compact and interpretable convolutional neural network for cross-subject driver drowsiness detection from single-channel EEG*. Methods, 2021.
6. Liang, Y., et al., *Explaining the black-box model: A survey of local interpretation methods for deep neural networks*. Neurocomputing, 2021. **419**: p. 168-182.
7. Zhang, Y., et al., *A survey on neural network interpretability*. IEEE Transactions on Emerging Topics in Computational Intelligence, 2021.
8. Samek, W., et al., *Explaining deep neural networks and beyond: A review of methods and applications*. Proceedings of the IEEE, 2021. **109**(3): p. 247-278.
9. Ancona, M., et al., *Towards better understanding of gradient-based attribution methods for deep neural networks*. arXiv preprint arXiv:1711.06104, 2017.
10. Simonyan, K., A. Vedaldi, and A. Zisserman. *Deep inside convolutional networks: Visualising image classification models and saliency maps*. in *In Workshop at International Conference on Learning Representations*. 2014. Citeseer.
11. Zeiler, M.D. and R. Fergus. *Visualizing and understanding convolutional networks*. in *European conference on computer vision*. 2014. Springer.
12. Springenberg, J.T., et al., *Striving for simplicity: The all convolutional net*. arXiv preprint arXiv:1412.6806, 2014.
13. Shrikumar, A., et al., *Not just a black box: Learning important features through propagating activation differences*. arXiv preprint arXiv:1605.01713, 2016.
14. Sundararajan, M., A. Taly, and Q. Yan. *Axiomatic attribution for deep networks*. in *International Conference on Machine Learning*. 2017. PMLR.
15. Bach, S., et al., *On pixel-wise explanations for non-linear classifier decisions by layer-wise relevance propagation*. PloS one, 2015. **10**(7): p. e0130140.
16. Petsiuk, V., A. Das, and K. Saenko, *Rise: Randomized input sampling for explanation of black-box models*. arXiv preprint arXiv:1806.07421, 2018.
17. Zintgraf, L.M., et al., *Visualizing deep neural network decisions: Prediction difference analysis*. arXiv preprint arXiv:1702.04595, 2017.
18. Fong, R.C. and A. Vedaldi. *Interpretable explanations of black boxes by meaningful perturbation*. in *Proceedings of the IEEE international conference on computer vision*. 2017.
19. Yuan, H., et al., *Interpreting image classifiers by generating discrete masks*. IEEE Transactions on Pattern Analysis and Machine Intelligence, 2020.
20. Hooker, S., et al., *A benchmark for interpretability methods in deep neural networks*. arXiv preprint arXiv:1806.10758, 2018.
21. Tjoa, E. and C. Guan, *Quantifying explainability of saliency methods in deep neural networks*. arXiv preprint arXiv:2009.02899, 2020.
22. Ismail, A.A., et al., *Benchmarking deep learning interpretability in time series predictions*. arXiv preprint arXiv:2010.13924, 2020.
23. Bang, J.-S., et al., *Spatio-spectral feature representation for motor imagery classification using convolutional neural networks*. IEEE Transactions on Neural Networks and Learning Systems, 2021.
24. Sturm, I., et al., *Interpretable deep neural networks for single-trial EEG classification*. Journal of neuroscience methods, 2016. **274**: p. 141-145.
25. Özdenizci, O., et al., *Learning invariant representations from EEG via adversarial inference*. IEEE access, 2020. **8**: p. 27074-27085.
26. Zhou, B., et al. *Learning deep features for discriminative localization*. in *Proceedings of the IEEE conference on computer vision and pattern recognition*. 2016.
27. Cui, J., et al. *Subject-Independent Drowsiness Recognition from Single-Channel EEG with an Interpretable CNN-LSTM model*. in *2021 International Conference on Cyberworlds (CW)*. 2021. IEEE.
28. Cui, J., et al. *EEG-based Cross-Subject Driver Drowsiness Recognition with an Interpretable Convolutional Neural Network*. 2021; Available from: <https://arxiv.org/abs/2107.09507>.
29. Mopuri, K.R., U. Garg, and R.V. Babu, *Cnn fixations: an unraveling approach to visualize the discriminative image regions*. IEEE Transactions on Image Processing, 2018. **28**(5): p. 2116-2125.
30. Ang, K.K., et al., *Filter bank common spatial pattern algorithm on BCI competition IV datasets 2a and 2b*. Frontiers in neuroscience, 2012. **6**: p. 39.
31. De Vries, S. and T. Mulder, *Motor imagery and stroke rehabilitation: a critical discussion*. Journal of rehabilitation medicine, 2007. **39**(1): p. 5-13.
32. *BCI Competition IV*. Available from: <http://www.bbci.de/competition/iv/#dataset2a>.
33. Margaux, P., et al., *Objective and subjective evaluation of online error correction during P300-based spelling*. Advances in Human-Computer Interaction, 2012. **2012**.

34. *BCI Challenge @ NER 2015*. 2015; Available from: <https://www.kaggle.com/c/inria-bci-challenge>.
35. Cao, Z., et al., *Multi-channel EEG recordings during a sustained-attention driving task*. Scientific data, 2019. **6**(1): p. 1-8.
36. Wei, C.-S., et al., *Toward drowsiness detection using non-hair-bearing EEG-based brain-computer interfaces*. IEEE transactions on neural systems and rehabilitation engineering, 2018. **26**(2): p. 400-406.
37. vlawhern. *Army Research Laboratory (ARL) EEGModels Project: A Collection of Convolutional Neural Network (CNN) models for EEG signal classification, using Keras and Tensorflow*. Available from: <https://github.com/vlawhern/arl-eeemodels>.
38. cuijiancorbin. *EEG-based-Cross-Subject-Driver-Drowsiness-Recognition-with-an-Interpretable-CNN*. 2021; Available from: <https://github.com/cuijiancorbin/EEG-based-Cross-Subject-Driver-Drowsiness-Recognition-with-an-Interpretable-CNN>.
39. Kingma, D.P. and J. Ba, *Adam: A method for stochastic optimization*. arXiv preprint arXiv:1412.6980, 2014.
40. Lin, M., Q. Chen, and S. Yan, *Network in network*. arXiv preprint arXiv:1312.4400, 2013.
41. Zhang, J., et al., *Top-down neural attention by excitation backprop*. International Journal of Computer Vision, 2018. **126**(10): p. 1084-1102.
42. Smilkov, D., et al., *Smoothgrad: removing noise by adding noise*. arXiv preprint arXiv:1706.03825, 2017.
43. Montavon, G., et al., *Explaining nonlinear classification decisions with deep taylor decomposition*. Pattern Recognition, 2017. **65**: p. 211-222.
44. Lundberg, S.M. and S.-I. Lee. *A unified approach to interpreting model predictions*. in *Proceedings of the 31st international conference on neural information processing systems*. 2017.
45. Xie, N., et al., *Explainable deep learning: A field guide for the uninitiated*. arXiv preprint arXiv:2004.14545, 2020.
46. Jesus, S., et al. *How can I choose an explainer? An Application-grounded Evaluation of Post-hoc Explanations*. in *Proceedings of the 2021 ACM Conference on Fairness, Accountability, and Transparency*. 2021.
47. Prasad, G., et al., *To what extent do human explanations of model behavior align with actual model behavior?* arXiv preprint arXiv:2012.13354, 2020.
48. Pfurtscheller, G. and F.L. Da Silva, *Event-related EEG/MEG synchronization and desynchronization: basic principles*. Clinical neurophysiology, 1999. **110**(11): p. 1842-1857.
49. Maezawa, H., *Cortical mechanisms of tongue sensorimotor functions in humans: A review of the magnetoencephalography approach*. Frontiers in human neuroscience, 2017. **11**: p. 134.
50. Miltner, W.H., C.H. Braun, and M.G. Coles, *Event-related brain potentials following incorrect feedback in a time-estimation task: evidence for a "generic" neural system for error detection*. Journal of cognitive neuroscience, 1997. **9**(6): p. 788-798.
51. Simon, M., et al., *EEG alpha spindle measures as indicators of driver fatigue under real traffic conditions*. Clinical Neurophysiology, 2011. **122**(6): p. 1168-1178.
52. Britton, J.W., et al., *Electroencephalography (EEG): An introductory text and atlas of normal and abnormal findings in adults, children, and infants*. 2016.
53. Da Silva, F.L., et al., *Models of neuronal populations: the basic mechanisms of rhythmicity*, in *Progress in brain research*. 1976, Elsevier. p. 281-308.
54. Borra, D., S. Fantozzi, and E. Magosso, *Interpretable and lightweight convolutional neural network for EEG decoding: application to movement execution and imagination*. Neural Networks, 2020. **129**: p. 55-74.